ACS OMEGA

Open Access

http://pubs.acs.org/journal/acsodf

Article

Tailoring Triuranium Octoxide into Multidimensional Uranyl Fluoride Micromaterials

Harry Jang and Frederic Poineau*

Cite This: *ACS Omega* 2024, 9, 26380−26387

Read Online

ACCESS | Metrics & More | Article Recommendations | Supporting Information

ABSTRACT: Uranium microstructured materials with controlled size and shape are relevant to the nuclear industry and have found applications as targets for medical isotope production, fuels for nuclear reactors, standards for nuclear forensics, and energy sources for space exploration. Until now, most studies at the microscale have focused on uranium microspheres (oxides, nitrides, carbides, and fluorides), while micromaterials of uranium halides, carbides, and pnictides with other morphologies are largely unknown. A promising method to shape the morphology of uranium micromaterials is the replacement of O by F atoms in oxide materials using a solid−gas reaction. Here, with the aim to elaborate unexplored uranium fluoride micromaterials, the fluorination of uranium oxide (U_3O_8 and UO_2) microspheres (ms), microrods (mr), and microplates (mp) in an autoclave at 250 °C with $HF_{(g)}$ (produced from the thermal decomposition of silver bifluoride (SBF)) and with ammonium bifluoride (ABF) was evaluated. We show that the reactions between U_3O_8 mr and U_3O_8 mp and SBF provided the most efficient way to elaborate mr and mp UO_2F_2 micromaterials in a high yield (∼90%). The resulting UO_2F_2 mr (length: 3−20 μm) and UO_2F_2 mp (width: 1−7.5 μm) exhibited a well-defined geometry that was identical to that of the U_3O_8 precursors. Agglomerated $(NH_4)_3UO_2F_5$ and UO_2F_2 ms (2−3.5 μm) were prepared from the reaction of U_3O_8 ms with ABF. It is noted that the reaction of UO_2 ms with SBF and ABF did not provide any uranium fluoride micromaterials. The successful preparation of uranium fluoride microstructures (ms, mr, and mp) developed here opens the way to novel actinide fluoride micromaterials.

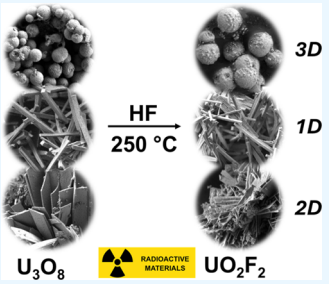

INTRODUCTION

The study of physicochemical phenomena at the microscale provides opportunities for the development of novel microstructured materials. One group of elements for which the diversity of microstructured materials is scarce is actinides. This state of fact is likely due to the radioactive nature of those elements and the small number of laboratories that can work with such materials. Uranium, the first actinide to be identified,[1] still has countless unexplored potential applications.

Uranium microstructured materials with controlled size and shape have found applications in several branches of the nuclear industry including as targets for medical isotope production,[2−4] fuels for nuclear reactors,[5−7] standards for nuclear forensics,[8−10] and energy sources for space exploration.[11] Morphological studies of actinide materials are also highly relevant to nuclear forensics-related work.[12,13] Potential applications include information storage, catalysis, sensors, and luminescent devices.[14−17] Most studies on uranium microstructured materials have focused on binary oxides, nitrides, carbides, and fluorides, with the spherical shape being the dominant morphology (Table 1). So far, aside from microspheres, microstructured uranium halide, carbide, and pnictide materials with other morphologies have not been reported. This paucity provides an opportunity for the development of novel materials with tunable catalytic and spectroscopic properties, as well as new nuclear fuels with increased gas retention and target materials with specific release rates of isotopes. In this context, the development of synthetic methods to control the chemical composition, size, and shape of uranium materials is of importance. So far, such methods are mostly hydrothermal or employ internal gelation (Table 1).

A promising method to tailor uranium micromaterials with controlled chemical composition, morphology, and size is chemical transformation. For transition metals and main group elements, chemical transformations have been used for the preparation of materials with energy applications.[30] For actinides, one simple chemical transformation is the replacement of O by F atoms in oxide materials using a solid−gas reaction.[31] Recently, we reported one such approach and prepared uranyl difluoride microspheres from the reaction of UO_3 ms and $HF_{(g)}$ produced from the decomposition of silver bifluoride (SBF).[29] The motivation for studying uranyl difluoride is that the material is relevant to nuclear and safeguard applications (e.g., as an intermediate for UF_6 and

Received: March 15, 2024
Revised: April 26, 2024
Accepted: May 29, 2024
Published: June 6, 2024

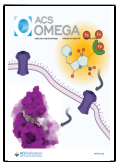

Table 1. Reported Microstructured Uranium Materials (ms: Microsphere, mr: Microrod, mp: Microplate)

material	shape	size	method (precursor)	reference
$3UO_3{\cdot}NH_3{\cdot}5H_2O$	ms	1.8 ± 0.1 μm	hydrothermal (UNH)[a]	18
	mr	4−10 μm length		
	mp	>5 μm length		
UO_3	ms	1.8 ± 0.1 μm	hydrothermal (UNH) and calcination ($3UO_3{\cdot}NH_3{\cdot}5H_2O$)	18
	ms	10−1000 μm	internal gelation (ADUN)#	19,20
U_3O_8	ms	1.8 ± 0.1 μm	hydrothermal (UNH) and calcination ($3UO_3{\cdot}NH_3{\cdot}5H_2O$)	18
	rod and plate microstructures	>2 μm	hydrothermal (uranyl acetate hydrate)	21
UO_2	ms	75−150 μm	internal gelation (ADUN)	22
	mr	400−800 μm	pellet annealing (U_3O_8)	23
U_2N_3	ms	1−2.5 μm	internal gelation (ADUN) and nitridation ($UO_3{\cdot}xH_2O$ + 2.65C)	24
UN	ms	1−2.5 μm	decomposition (U_2N_3)	24
	ms	∼800 μm	internal gelation (ADUN) and carbothermic reduction (UO_2)	25
	ms	∼825 μm	internal gelation (ADUN) and carbothermic conversion ($UO_3{\cdot}2H_2O$)	26
UC	ms	675 ± 10 μm	internal gelation (ADUN), calcination ($UO_3{\cdot}2H_2O$), and carbothermic reduction (UO_2)	27
UF_4	ms	∼15 μm	hydrofluorination with HF (UO_2)	28
UO_2F_2	ms	1−2 μm	hydrothermal (UNH), calcination, ($3UO_3{\cdot}NH_3{\cdot}5H_2O$), and fluorination with SBF (UO_3)	29

[a]UNH: uranyl nitrate hexahydrate. #ADUN: acid-deficient uranyl nitrate.

UO_2 conversion).[32−34] Also, fluorinated U materials (UO_2F_2, UF_4) exhibit photoluminescent properties[35,36] that are studied to improve radiation detection technology, such as the detection of leaking UF_6 cylinders[37] and sensitive low-dose measurements.[38]

Uranium fluoride mr and mp have not yet been reported (vide supra). The reactions of UO_2 and U_3O_8 with NH_4HF_2 (ABF) lead to several uranium fluoride compounds, respectively ($(NH_4)_4UF_8$, $(NH_4)_2UF_6$, UF_4)[39,40] and ($(NH_4)_3UO_2F_5$ and UO_2F_2).[39,41] These reactions have been well studied for bulk materials but not for well-defined micromaterials. Due to the importance of ABF in actinide synthetic chemistry[39−44] and uranium oxides in the nuclear industry, here we expand our efforts and investigate the preparation of ms, mr, and mp uranium fluoride micromaterials via the reaction of UO_2 ms and U_3O_8 ms, mr, and mp with SBF and ABF.

RESULTS AND DISCUSSION

Uranium oxide precursors with well-defined shapes and sizes are key to the preparation of uranium fluoride micromaterials with a controlled geometry. Based on previous results with MoS_2 nanostructures and UO_2F_2 ms (vide supra), it is expected that the shape of the precursors will be retained during the chemical transformations investigated here.

The uranium precursors (U_3O_8 ms, mr, mp, and UO_2 ms; see the Experimental Methods section) were characterized by scanning electron microscopy (SEM) and powder X-ray diffraction (PXRD). The PXRD results confirm the presence of α-U_3O_8 and UO_2 (respectively, Figures S1 and S2, Supporting Information). The SEM analysis (Figure 1) indicates that the size and shape of U_3O_8 ms (1−2 μm) and mr (3−27 μm) are consistent with the one obtained by Wang et al.,[18] while U_3O_8 mp exhibits a completely different morphology than the disc-like ones reported. SEM analysis shows the U_3O_8 mp to agglomerate into large clusters (Figure S3, Supporting Information), and the dimensions of these plates vary drastically (1−6 μm in width) between clusters. Possible explanations for this discrepancy are the volume (and consequently pressure) of the autoclave used in our study (23 mL) compared to that of Wang et al. (12.5 mL), and the larger scales performed in our work (2−4 times greater than those of Wang et al.). Formation of these structures is dictated by the favored and suppressed growth along crystallographic directions,[45−47] and the modifications in volume and concentration may have impacted these formations. Our material may have initially formed like a star with growth surfaces in many directions, which then each formed rectangular ends along another direction, whereas the plates from Wang et al. likely formed with growth already suppressed in one direction.

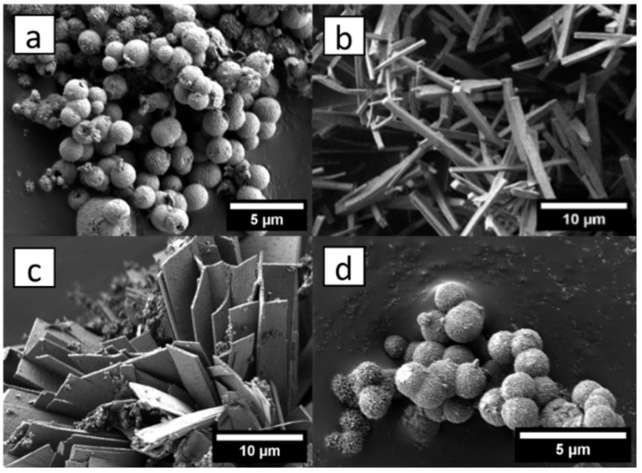

Figure 1. SEM images of (a) U_3O_8 ms (13,200×), (b) U_3O_8 mr (7420×), (c) U_3O_8 mp (7790×), and (d) UO_2 ms (18,400×) precursors.

U_3O_8 microplates have already been reported and were formed from the thermal decomposition of uranyl ammonium carbonate.[48−51] U_3O_8 mp reported here could be used as precursors to prepare several other uranium oxide materials (UO_2, UO_3) with a rectangular geometry, enabling investigations on the effects of morphology (i.e., mp vs ms) of uranium oxides on several physicochemical properties (i.e., catalysis).

https://doi.org/10.1021/acsomega.4c02554
ACS Omega 2024, 9, 26380−26387

The successful preparation of mr and mp UO_2F_2 micromaterials involves the fluorination of U_3O_8 with SBF at 250 °C (eq 1; see the Experimental Methods section). The reaction between U_3O_8 mr and mp with SBF at 250 °C yields UO_2F_2 mr and mp in high yields of 96.5 and 94.9%, respectively (see eq S1). The SEM analysis indicates that the resulting UO_2F_2 mr and mp exhibit well-defined morphologies with shapes and surface smoothness similar to those of their respective U_3O_8 precursor. Size distribution analysis indicates that the length of the rods varies predominantly from 3 to 20 μm (Figure 2d) and the width of the plates varies from 1 to 7.5 μm (Figure 3d).

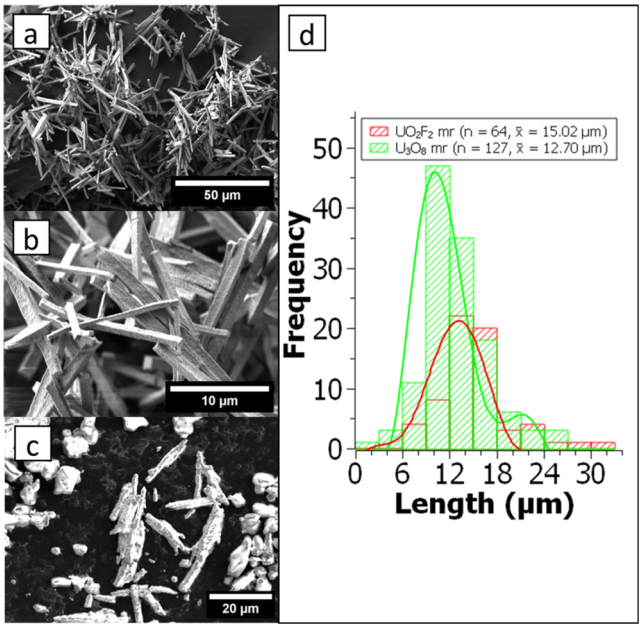

Figure 2. SEM images of UO_2F_2 mr at (a) 1910× and (b) 10,100× obtained using U_3O_8 mr and SBF, (c) $(NH_4)_3UO_2F_5$ mr (3180×) using U_3O_8 mr and ABF, and (d) particle size distribution of lengths of U_3O_8 mr and UO_2F_2 mr.

During the reaction with SBF ($HF_{(g)}$ acting as the fluorinating agent), the mr or mp morphologies of the U_3O_8 precursors were well-conserved with no geometrical distortions/transformations, consistent with other gas−solid chemical transformations performed at the nanoscale. One example of such chemical transformation is the conversion of MoO_3 to MoS_2 nanostructures by a solid−gas reaction using H_2S gas.[30,52] In this type of reaction, the size and shape of the oxide precursors determine the morphology of the sulfide reaction product. It was shown that MoS_2 nanoribbons were prepared from the reaction of the MoO_3 nanoribbon reaction at 800 °C in a $H_2S/H_2/N_2$ atmosphere.[53]

Using ABF as the fluorinating agent, the reaction between U_3O_8 mr and ABF led to a $(NH_4)_3UO_2F_5$ material that did not retain the smoothness and shape of the U_3O_8 mr precursor (Figure 2c). The decomposition of $(NH_4)_3UO_2F_5$ produced a material consisting of large particles (5−15 μm) (Figure S4, Supporting Information). Reactions between U_3O_8 mp and ABF produced large clusters (>10 μm) of $(NH_4)_3UO_2F_5$ resembling pebble-like particles (Figure 3c), and rougher surfaces were observed when decomposed at 300 °C (Figure S5, Supporting Information). This study shows that for the preparation of mr or mp materials, the nature of the

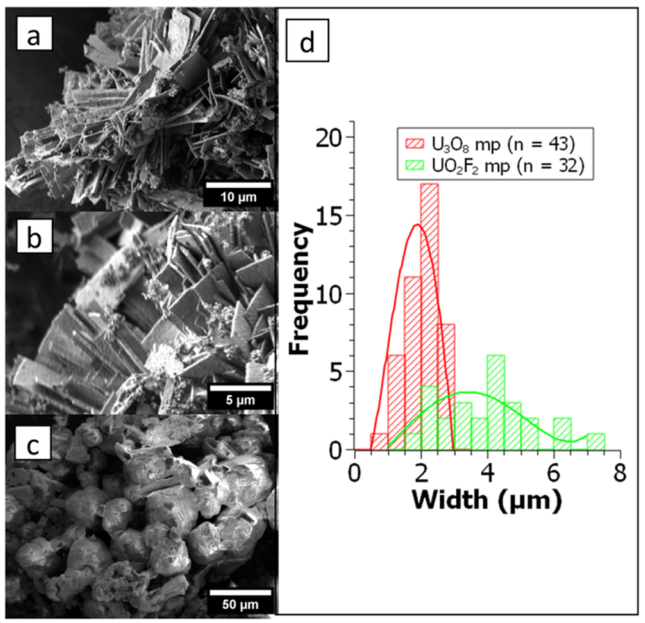

Figure 3. SEM images of UO_2F_2 mp at (a) 6580× and (b) 12,500× obtained using U_3O_8 mp and SBF, (c) large particles of $(NH_4)_3UO_2F_5$ (1250×) using ABF, and (d) particle size distribution of U_3O_8 mp and UO_2F_2 mp.

fluorinating agent has a profound effect on the morphology of the final uranium fluoride material.

UO_2F_2 ms has already been reported and was prepared from the reaction of UO_3 ms with SBF.[29] Here, we report the formation of UO_2F_2 ms by two other routes: the reactions of U_3O_8 ms with ABF and SBF.

The reaction of U_3O_8 ms with SBF at 250 °C (eq 1, see the Experimental Methods section) produced UO_2F_2 ms with an average size of 2.7 μm, larger than those previously prepared from UO_3 ms and SBF (1−2 μm) (Figure 4a). The reaction between U_3O_8 ms and ABF produced agglomerated $(NH_4)_3UO_2F_5$ ms (Figure 4b). It was hypothesized that the agglomeration phenomenon is due to the condensation and reaction of NH_4F on UO_2F_2 ms (eq 2). Further decomposition of $(NH_4)_3UO_2F_5$ ms at 300 °C led to UO_2F_2 ms (eq 3, Figure 4c). The morphology of UO_2F_2 ms (2−3.5 μm) obtained from $(NH_4)_3UO_2F_5$ ms consists of swollen hollow spheroid particles with a rough surface. This morphology was completely different from the one obtained from the reaction of UO_3 ms or U_3O_8 ms with SBF, so these morphological differences could be utilized for nuclear forensic purposes. The particle size distribution analysis (Figure 4d) indicates that UO_2F_2 ms obtained from the fluorination with $HF_{(g)}$ and the decomposition of $(NH_4)_3UO_2F_5$ have approximately the same size and are both 1 μm larger than the U_3O_8 ms precursors.

Finally, the reaction between UO_2 ms with ABF (eq 4) yielded $(NH_4)_2UF_6$ (Figure S6, Supporting Information). During this reaction, the spherical geometry was entirely lost, likely due to the susceptibility of tetravalent uranium fluoride to hydrolysis[28,40] combined with the agglomerating effect of NH_4F

https://doi.org/10.1021/acsomega.4c02554
ACS Omega 2024, 9, 26380−26387

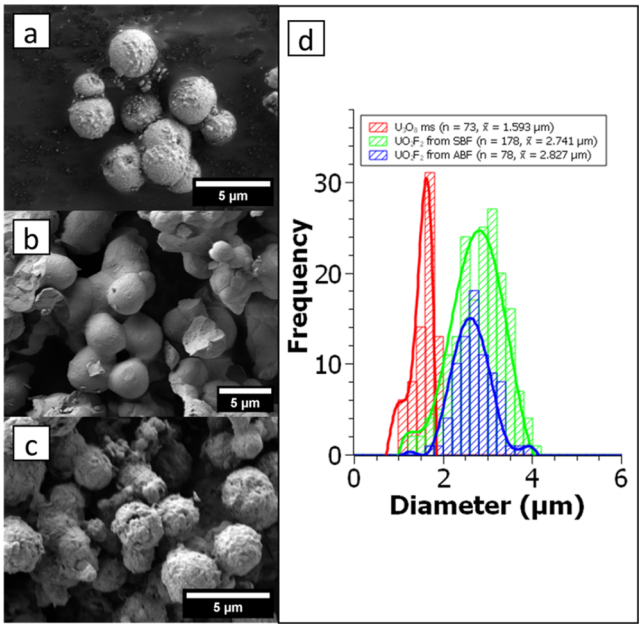

Figure 4. SEM images of (a) UO_2F_2 ms (15,100×) prepared from the reaction of U_3O_8 ms with SBF, (b) $(NH_4)_3UO_2F_5$ ms (10,500×) prepared from the reaction of U_3O_8 ms with ABF, (c) UO_2F_2 ms (16,900×) prepared from the decomposition of panel (b), and (d) particle size distribution of U_3O_8 ms and UO_2F_2 ms (a, c).

$$U_3O_8(s) + 6HF(g) + \frac{1}{2}O_2(g) \rightarrow 3UO_2F_2(s) + 3H_2O(g)(T = 250\ ^\circ C) \quad (1)$$

$$UO_2F_2(s) + 3NH_4F(g) \rightarrow (NH_4)_3UO_2F_5(s)(T = 250\ ^\circ C) \quad (2)$$

$$(NH_4)_3UO_2F_5(s) \rightarrow UO_2F_2(s) + 3NH_4F(g)(T = 300\ ^\circ C) \quad (3)$$

$$UO_2(s) + 2NH_4F + 4HF \rightarrow (NH_4)_2UF_6(s) + 2H_2O(g)(T = 250\ ^\circ C) \quad (4)$$

CONCLUSIONS

In summary, with the aim to elaborate on uranium fluoride micromaterials with controlled shapes and sizes, the fluorination of uranium oxides (ms, mr, and mp) with SBF and ABF was evaluated. U_3O_8 micromaterials were successfully fluorinated, and $(NH_4)_3UO_2F_5$ ms and UO_2F_2 mp and mr were observed. The reaction between U_3O_8 and SBF provided the most efficient way to elaborate mr and mp micromaterials. The UO_2F_2 mr and mp exhibited a geometry identical to that of its U_3O_8 precursor, with no signs of deformation with smooth surfaces and well-defined angles. It is noted that the reaction of UO_2 at milliseconds with SBF and ABF did not provide any satisfactory results. These UO_2F_2 materials could be used to evaluate the morphological effects on UO_2F_2 photoluminescent properties for radiation detection application and calibrate equipment for fingerprint analysis for environmental remediation and nuclear forensics application. On the fundamental side, UO_2F_2 ms, mp, and mr could be used as precursors to expand the library of available uranium micromaterials, one example being $[UO_2F_2(NH_3)_3]_2{\cdot}2NH_3$.[54] Future research will also explore the fluorination of uranium oxide nanomaterials with controlled geometry. It is expected that at the nanoscale, the large surface area would enhance the reactivity of the materials and may enable UO_2 nanospheres, nanorods, and nanoplates to be converted to UF_4 of respective morphologies at $T < 250\ ^\circ C$.[55] Finally, the successful preparation of uranium fluoride ms, mp, and mr presented here can pave the way for the development of other actinide fluoride micromaterials with those morphologies.

EXPERIMENTAL METHODS

Caution! Uranium-238 is an α emitter (E_{max} = 4.26 MeV). All manipulations were performed in a designed radiochemistry laboratory equipped with HEPA filter hoods and by following approved radioisotope handling and monitoring procedures.

Materials and Methods. Silver bifluoride (≥99%, Alfa Aesar), ammonium bifluoride (≥99%, Alfa Aesar), glycerol (≥99.5%, Sigma-Aldrich), and urea (≥98%, Sigma-Aldrich) were used as received. $UO_2(NO_3)_2{\cdot}6H_2O$ (UNH) was prepared from treatment with a uranium metal dissolved in hot nitric acid followed by recrystallization. The α-U_3O_8 polymorph was obtained for all of the U_3O_8 micromaterials (Figure S1, Supporting Information).[56]

Fluorination and hydrothermal reactions were conducted within a Parr model 4749 autoclave placed in a Thermo Scientific Thermolyne Benchtop muffle furnace (model FB1315M). All of the fluorination reactions involving U_3O_8, UO_2, ABF, and SBF were conducted at 250 °C for 24 h in the setup reported in Figure S7 (Supporting Information). Reactions of U_3O_8 materials were performed in a fume hood in the presence of air, while reactions involving UO_2 were performed in a glovebox under a dry N_2 atmosphere. Uranium fluorides have been observed to react with nitrogen to form uranium nitrides at high temperatures (>800 °C) in the presence of reducing materials (e.g., Si).[57] In our experimental conditions (250 °C and absence of reducing materials), the formation of uranium nitrides is not expected. Additionally, the formation of UF_4 from the hydrofluorination of UO_2 in a nitrogen atmosphere is the most thermodynamically favorable reaction.[58,59]

At 250 °C, the gaseous decomposition product(s) of SBF ($HF_{(g)}$) and ABF ($HF_{(g)}$ and $NH_4F_{(g)}$) provide the source of fluorine for the reactions. In those reactions, the SBF or ABF salt in excess molar quantity was placed on the Teflon liner of the vessel, while the uranium oxide material was placed in a 15 mL Teflon vial above the bifluoride salt (Figure S7, Supporting Information). $(NH_4)_3UO_2F_5$ was decomposed in a Teflon vial by thermal treatment in a benchtop muffle furnace. A summary of the reactions investigated is presented in Figure 5.

Powder X-ray diffraction measurements were performed at room temperature on a Bruker D8 Advanced diffractometer equipped with Cu Kα X-rays (λ = 1.5406 Å) and a solid-state Si detector. Imaging was performed on the JEOL Tescan CLARA field emission scanning electron microscope, and samples were mounted on carbon tape without coating. Particle sizes were measured using ImageJ, and particle size distribution figures were generated using SciDAVis.

Preparation of U_3O_8 ms. $3UO_3{\cdot}NH_3{\cdot}5H_2O$ ms was prepared using a modified version of the reported method.[18] UNH (620.5 mg) was dissolved and hand-stirred in a mixture of water (6.0 mL), glycerol (4.5 mL), and urea (225.4 mg) in

https://doi.org/10.1021/acsomega.4c02554
ACS Omega 2024, 9, 26380−26387

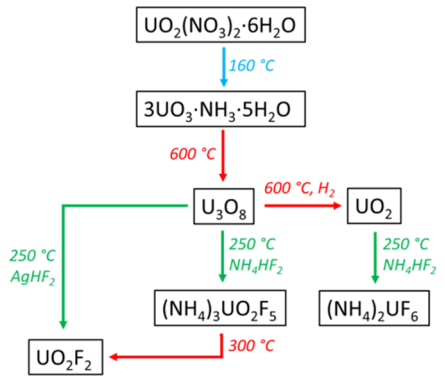

Figure 5. Summary of the chemical reactions explored. Experiments were conducted in air except for reduction to UO_2. Blue, hydrothermal process; red, thermal treatment; and green, fluorination in autoclave.

an autoclave under air, placed in a furnace, treated at 160 °C for 5 h, and allowed to cool for 2 h prior to opening. Following the reaction, the resulting yellow precipitate was transferred to a 15 mL centrifuge tube, washed and centrifuged with water (10 mL) and ethanol (10 mL) 3×, and dried in air at 60 °C overnight. The resulting $3UO_3{\cdot}NH_3{\cdot}5H_2O$ ms product (328.6 mg, 82.6% yield) was collected (Figure S8, Supporting Information).

$3UO_3{\cdot}NH_3{\cdot}5H_2O$ milliseconds was treated at 600 °C for 3 h under air. Following the reaction, the U_3O_8 ms (255.3 mg, 73.6% yield from UNH) was characterized by SEM (Figure 1a) and PXRD (Figure S1, Supporting Information). PXRD showed the presence of α-U_3O_8.

Preparation of U_3O_8 mr. $3UO_3{\cdot}NH_3{\cdot}5H_2O$ mr was prepared using the reported method.[18] UNH (390.3 mg) was dissolved and hand-stirred in a mixture of water (4.0 mL), glycerol (8.0 mL), and urea (52.8 mg) in an autoclave under air, placed in a furnace, treated at 160 °C for 3 h (to avoid glycerol degradation), and allowed to cool for 2 h prior to opening. Following the reaction, the resulting yellow precipitate was transferred to a 15 mL centrifuge tube, washed and centrifuged with water (10 mL) and ethanol (10 mL) 3×, and dried under air at 60 °C overnight. The resulting $3UO_3{\cdot}NH_3{\cdot}5H_2O$ mr product (228.7 mg, 91.5% yield) was collected.

$3UO_3{\cdot}NH_3{\cdot}5H_2O$ mr was treated at 600 °C for 3 h under air. Following the reaction, the U_3O_8 mr (160.4 mg, 73.5% from UNH) was characterized by SEM (Figure 1b) and PXRD (Figure S1, Supporting Information).

Preparation of U_3O_8 mp. $3UO_3{\cdot}NH_3{\cdot}5H_2O$ mp was prepared according to the reported method.[18] UNH (814.2 mg) was dissolved and hand-stirred in a mixture of water (8.0 mL) and urea (303.6 mg) in an autoclave under air, placed in a furnace, treated at 160 °C for 5 h, and allowed to cool for 2 h prior to opening. Following the reaction, the resulting yellow precipitate was transferred to a 15 mL centrifuge tube, washed and centrifuged with water (10 mL) and ethanol (10 mL) 3×, and dried under air at 60 °C overnight. The resulting $3UO_3{\cdot}NH_3{\cdot}5H_2O$ mp product (493.6 mg, 94.6% yield) was collected.

$3UO_3{\cdot}NH_3{\cdot}5H_2O$ mp was treated at 600 °C for 3 h under air. Following the reaction, the U_3O_8 mp (288.5 mg, 63.4% yield from UNH) was characterized by SEM (Figure 1a) and PXRD (Figure S1, Supporting Information). PXRD results show the presence of α-U_3O_8.

Preparation of UO_2 ms. UO_2 ms (Figure S2, Supporting Information) was prepared by the thermal treatment of U_3O_8 ms (246.8 mg) at 600 °C for 5 h in 5% H_2/95% Ar gas using a Thermo Scientific Lindberg/Blue M Mini-Mite tube furnace, similar to a previously reported setup.[60] The resulting UO_2 ms (223.0 mg, 93.9% yield) was characterized by SEM and PXRD (Figure S2, Supporting Information).

Preparation of UO_2F_2 ms from U_3O_8 ms. U_3O_8 milliseconds (41.6 mg) in a Teflon vial was placed in a Teflon liner of the autoclave containing SBF (193.1 mg). The autoclave was then sealed and treated at 250 °C for 24 h in a muffle furnace. Following the reaction, the autoclave was cooled for 2 h to room temperature and opened, and the resulting yellow-green UO_2F_2 ms product (44.4 mg, 97.3% yield) was collected and characterized by PXRD (Figure S9, Supporting Information) and SEM (Figure 4a).

Preparation of UO_2F_2 mr from U_3O_8 mr. U_3O_8 mr (32.5 mg) in a Teflon vial was placed in a Teflon liner of the autoclave containing SBF (217.1 mg). The autoclave was then sealed and treated at 250 °C for 24 h in a muffle furnace. Following the reaction, the autoclave was cooled for 2 h to room temperature and opened, and the resulting yellow-green UO_2F_2 mr product (34.4 mg, 96.5% yield) was collected and characterized by PXRD (Figure S9, Supporting Information) and SEM (Figure 2a).

Preparation of UO_2F_2 mp from U_3O_8 mp. U_3O_8 mp (21.7 mg) in a Teflon vial was placed in a Teflon liner of the autoclave containing SBF (148.1 mg). The autoclave was then sealed and treated at 250 °C for 24 h in a muffle furnace. Following the reaction, the autoclave was cooled for 2 h to room temperature and opened, and the resulting yellow-green UO_2F_2 mp product (22.6 mg, 94.9% yield) was collected and characterized by PXRD (Figure S9, Supporting Information) and SEM (Figure 3a).

Preparation of $(NH_4)_3UO_2F_5$ ms from U_3O_8 ms. U_3O_8 milliseconds (51.4 mg) in a Teflon vial was placed in a Teflon liner of the autoclave containing ABF (206.1 mg). Following the reaction, the autoclave was cooled for 2 h to room temperature and opened, and the resulting green $(NH_4)_3UO_2F_5$ ms product (72.6 mg, 94.5% yield) was collected and characterized by PXRD (Figure S10, Supporting Information) and SEM (Figure 4b).

Preparation of $(NH_4)_3UO_2F_5$ mr from U_3O_8 mr. U_3O_8 mr (31.7 mg) in a Teflon vial was placed in a Teflon liner of the autoclave containing ABF (124.8 mg). Following the reaction, the autoclave was cooled for 2 h to room temperature and opened, and the resulting green $(NH_4)_3UO_2F_5$ mr product (46.0 mg, 97.2% yield) was collected and characterized by PXRD (Figure S10, Supporting Information) and SEM (Figure 2b).

Preparation of $(NH_4)_3UO_2F_5$ mp from U_3O_8 mp. U_3O_8 mp (23.7 mg) in a Teflon vial was placed in a Teflon liner of the autoclave containing ABF (203.6 mg). Following the reaction, the autoclave was cooled for 2 h to room temperature and opened, and the resulting green $(NH_4)_3UO_2F_5$ mp product (29.4 mg, 83.1% yield) was collected and characterized by PXRD (Figure S10, Supporting Information) and SEM (Figure 3b).

Preparation of UO_2F_2 ms from $(NH_4)_3UO_2F_5$ ms. $(NH_4)_3UO_2F_5$ ms (28.1 mg) was placed in a Teflon vial and treated at 300 °C for 24 h in a furnace. The resulting yellow UO_2F_2 ms (17.0 mg, 82.3% yield) was cooled for 2 h to room temperature and characterized by SEM (Figure 4c) and PXRD (Figure S10, Supporting Information).

https://doi.org/10.1021/acsomega.4c02554
ACS Omega 2024, 9, 26380−26387

Preparation of $(NH_4)_2UF_6$ ms from UO_2 ms. UO_2 ms (84.9 mg) (Figure S2, Supporting Information) in a Teflon vial was placed in a Teflon liner of the autoclave containing ABF (217.9 mg). The autoclave was sealed, removed from the glovebox, placed in a furnace, and treated at 250 °C for 24 h. Following the reaction, the autoclave was cooled for 2 h to room temperature, transferred back to the glovebox, opened, and the resulting green $(NH_4)_2UF_6$ ms product (120.9 mg, 99.0% yield) was collected and characterized by PXRD and SEM (Figure S6, Supporting Information).

■ ASSOCIATED CONTENT

Supporting Information

The Supporting Information is available free of charge at https://pubs.acs.org/doi/10.1021/acsomega.4c02554.

Additional SEM results, powder X-ray diffraction data, and particle size data (PDF)

■ AUTHOR INFORMATION

Corresponding Author

Frederic Poineau − *Department of Chemistry and Biochemistry, University of Nevada Las Vegas, Las Vegas, Nevada 89154, United States;* orcid.org/0000-0002-9517-2264; Email: poineauf@unlv.nevada.edu

Author

Harry Jang − *Department of Chemistry and Biochemistry, University of Nevada Las Vegas, Las Vegas, Nevada 89154, United States*

Complete contact information is available at: https://pubs.acs.org/10.1021/acsomega.4c02554

Author Contributions

The manuscript was written through contributions of all authors. H.J.: investigation, methodology, writing, review, and editing. F.P.: conceptualization, writing, review, and funding acquisition.

Funding

This material is based upon work performed under the auspices of the Consortium on Nuclear Security Technologies (CONNECT) supported by the Department of Energy/National Nuclear Security Administration under Award Number(s) DE-NA0003948.

Notes

The authors declare no competing financial interest.

■ ACKNOWLEDGMENTS

The authors would like to thank Wendee Johns for administrative support and Quinn Summerfield for laboratory support.

■ ABBREVIATIONS

ms, microspheres; mr, microrods; mp, microplates; SBF, silver bifluoride ($AgHF_2$); ABF, ammonium bifluoride (NH_4HF_2); SEM, scanning electron microscopy; XRD, X-ray diffraction; UNH, uranyl nitrate hexahydrate; ADUN, acid-deficient uranyl nitrate

■ REFERENCES

(1) Morrison, J. M. Uranium—History of an Element. In *Uranium: Cradle to Grave*; Mineralogical Association of Canada, 2013.

(2) Henry, R.; Saclay, H. The Use of Recoil for the Separation of Uranium Fission Products. In *Utilisation du recul pour la separation des produits de fission de l'uranium*; Centre d'études nucléaires: France, 1959.

(3) Passy, U.; Steiger, N. H. Some Nuclear-Chemical and Physicochemical Problems in Fission-Product Recoil Separation. *Nucl. Sci. Eng.* **1963**, *15* (4), 366−374.

(4) Dorhout, J. M.; Wilkerson, M. P.; Czerwinski, K. R. Irradiation and Isolation of Fission Products from Uranium Metal−Organic Frameworks. *J. Radioanal. Nucl. Chem.* **2019**, *320* (2), 415−424.

(5) Khanal, L. R.; Sundararajan, J. A.; Qiang, Y. Advanced Nanomaterials for Nuclear Energy and Nanotechnology. *Energy Technol.* **2020**, *8* (3), No. 1901070.

(6) Filippov, E. A.; Karelin, A. I.; Lobas, O. P.; Papkov, A. S.; Zhiganov, A. N.; Mishina, L. A.; Shamin, V. I. State and Tendency of Developing Physical-Chemical Methods for Making Actinide Microspherical Particles. *J. Radioanal. Nucl. Chem.* **1990**, *143* (1), 53−60.

(7) Robisson, A. C.; Lemonnier, S.; Granjean, S. *Sol Gel Chemistry Applied to the Synthesis of Actinide-Based Compounds for the Fabrication of Advanced Fuels*; INIS-FR-2925; CEA/VALRHO, 2004; pp 1−4.

(8) Middendorp, R.; Dürr, M.; Bosbach, D. The Stability of Uranium Microspheres for Future Application as Reference Standard in Analytical Measurements. *Proc. Chem.* **2016**, *21*, 285−292.

(9) Richter, S.; Truyens, J.; Venchiarutti, C.; Aregbe, Y.; Middendorp, R.; Neumeier, S.; Kegler, P.; Klinkenberg, M.; Zoriy, M.; Stadelmann, G.; Macsik, Z.; Koepf, A.; Sturm, M.; Konegger-Kappel, S.; Venzin, A.; Sangely, L.; Tanpraphan, T. Certification of the First Uranium Oxide Micro-Particle Reference Materials for Nuclear Safety and Security, IRMM-2329P and IRMM-2331P. *J. Radioanal. Nucl. Chem.* **2022**, *332*, 2809−2813.

(10) Kegler, P.; Pointurier, F.; Rothe, J.; Dardenne, K.; Vitova, T.; Beck, A.; Hammerich, S.; Potts, S.; Faure, A. L.; Klinkenberg, M.; Kreft, F.; Niemeyer, I.; Bosbach, D.; Neumeier, S. Chemical and Structural Investigations on Uranium Oxide-Based Microparticles as Reference Materials for Analytical Measurements. *MRS Adv.* **2021**, *6* (4−5), 125−130.

(11) Carmack, W. J.; Richardson, W. C.; Husser, D. L.; Mohr, T. C. Internal Gelation as Applied to the Production of Uranium Nitride Space Nuclear Fuel. *AIP Conf. Proc.* **2004**, *699*, 420−425.

(12) Schwerdt, I. J.; Hawkins, C. G.; Taylor, B.; Brenkmann, A.; Martinson, S.; McDonald, L. W. Uranium Oxide Synthetic Pathway Discernment through Thermal Decomposition and Morphological Analysis. *Radiochim. Acta* **2019**, *107* (3), 193−205.

(13) McDonald, L. W.; Sentz, K.; Hagen, A.; Chung, B. W.; Nizinski, C. A.; Schwerdt, I. J.; Hanson, A.; Donald, S.; Clark, R.; Sjoden, G.; Porter, R.; Athon, M. T.; Tasdizen, T.; Noel, V.; Webb, S. M.; Van Veelen, A.; Hickam, S. M.; Ly, C. Review of Multi-Faceted Morphologic Signatures of Actinide Process Materials for Nuclear Forensic Science. *J. Nucl. Mater.* **2024**, *588*, No. 154779.

(14) Pradhan, M.; Sarkar, S.; Sinha, A. K.; Basu, M.; Pal, T. Morphology Controlled Uranium Oxide Hydroxide Hydrate for Catalysis, Luminescence and SERS Studies. *CrystEngComm* **2011**, *13* (8), 2878−2889.

(15) Xu, C. X.; Sun, X. W.; Dong, Z. L.; Cui, Y. P.; Wang, B. P. Nanostructured Single-Crystalline Twin Disks of Zinc Oxide. *Cryst. Growth Des.* **2007**, *7* (3), 541−544.

(16) Zhang, Y. W.; Sun, X.; Si, R.; You, L. P.; Yan, C. H. Single-Crystalline and Monodisperse LaF_3 Triangular Nanoplates from a Single-Source Precursor. *J. Am. Chem. Soc.* **2005**, *127* (10), 3260−3261.

(17) Kim, C.; Kim, Y. J.; Jang, E. S.; Yi, G. C.; Kim, H. H. Whispering-Gallery-Modelike-Enhanced Emission from ZnO Nanodisk. *Appl. Phys. Lett.* **2006**, *88*, No. 093104.

(18) Wang, L.; Zhao, R.; Wang, C. Z.; Yuan, L. Y.; Gu, Z. J.; Xiao, C. L.; Wang, S. A.; Wang, X. W.; Zhao, Y. L.; Chai, Z. F.; Shi, W. Q. Template-Free Synthesis and Mechanistic Study of Porous Three-Dimensional Hierarchical Uranium-Containing and Uranium Oxide Microspheres. *Chem. - Eur. J.* **2014**, *20* (39), 12655−12662.

(19) Hunt, R. D.; Lindemer, T. B.; Hu, M. Z.; Del Cul, G. D.; Collins, J. L. Preparation of Spherical, Dense Uranium Fuel Kernels with Carbon. *Radiochim. Acta* **2007**, *95* (4), 225−232.
(20) Hunt, R. D.; Collins, J. L.; Lloyd, M. H.; Finkeldei, S. C. Production of More Ideal Uranium Trioxide Microspheres for the Sol-Gel Microsphere Pelletization Process without the Use of Carbon. *J. Nucl. Mater.* **2019**, *515*, 107−110.
(21) Yan, Q.; Mao, Y.; Zhou, X.; Liang, J.; Peng, S.; Ye, M. Control of the Compositions and Morphologies of Uranium Oxide Nanocrystals in the Solution Phase: Multi-Monomer Growth and Self-Catalysis. *Nanoscale Adv.* **2019**, *1* (4), 1314−1318.
(22) Hunt, R. D.; Hickman, R. R.; Ladd-Lively, J. L.; Anderson, K. K.; Collins, R. T.; Collins, J. L. Production of Small Uranium Dioxide Microspheres for Cermet Nuclear Fuel Using the Internal Gelation Process. *Ann. Nucl. Energy* **2014**, *69*, 139−143.
(23) Yang, J. H.; Rhee, Y. W.; Kim, D.; Kim, J. H.; Kang, K. W.; Kim, K. S. In *Fabrication of UO2+x Single Crystal Rods*, Transactions of the Korean Nuclear Society Autumn Meeting, Gyeongju, Korea, 2006; pp 1−2.
(24) Silva, C. M.; Hunt, R. D.; Snead, L. L.; Terrani, K. A. Synthesis of Phase-Pure U_2N_3 Microspheres and Its Decomposition into UN. *Inorg. Chem.* **2015**, *54* (1), 293−298.
(25) Ledergerber, G.; Kopajtic, Z.; Ingold, F.; Stratton, R. W. Preparation of Uranium Nitride in the Form of Microspheres. *J. Nucl. Mater.* **1992**, *188* (C), 28−35.
(26) Lindemer, T. B.; Voit, S. L.; Silva, C. M.; Besmann, T. M.; Hunt, R. D. Carbothermic Synthesis of 820 μm Uranium Nitride Kernels: Literature Review, Thermodynamics, Analysis, and Related Experiments. *J. Nucl. Mater.* **2014**, *448* (1−3), 404−411.
(27) Tian, W.; Guo, H.; Chen, D.; Pouchon, M. A.; Horwege, A.; Yin, X.; Huang, Q.; Wang, J.; Cao, S.; Chen, D.; Bai, J.; Tan, C.; Fan, F.; Wu, X.; Shen, T.; Qin, Z. Preparation of UC Ceramic Nuclear Fuel Microspheres by Combination of an Improved Microwave-Assisted Rapid Internal Gelation with Carbothermic Reduction Process. *Ceram. Int.* **2018**, *44* (15), 17945−17952.
(28) Foley, B. J.; Christian, J. H.; Klug, C. A.; Villa-Aleman, E.; Wellons, M. S.; DeVore, M.; Groden, N.; Darvin, J. Probing the Hydrolytic Degradation of UF_4 in Humid Air. *Dalton Trans.* **2022**, *51* (15), 6061−6067.
(29) Jang, H.; Louis-Jean, J.; Poineau, F. Synthesis and Morphological Control of UO_2F_2 Particulates. *ACS Omega* **2023**, *8*, 21996−22002.
(30) Moon, G. D.; Ko, S.; Min, Y.; Zeng, J.; Xia, Y.; Jeong, U. Chemical Transformations of Nanostructured Materials. *Nano Today* **2011**, *6* (2), 186−203.
(31) Katz, J. J.; Sheft, I. Halides Of The Actinide Elements. *Adv. Inorg. Chem. Radiochem.* **1960**, *2*, 195−236.
(32) Pastoor, K. J. Nuclear Forensics of Uranium Conversion: Investigations of Environmentally Altered Uranium Compounds. Ph.D. Dissertation, Colorado School of Mines: Golden, CO, 2021.
(33) Hou, R.; Mahmud, T.; Prodromidis, N.; Roberts, K. J.; Williams, R. A.; Goddard, D. T.; Semeraz, T. Synthesis of UO_2F_2 Nanoparticles in a Tubular Aerosol Reactor: Reactor Design and Experimental Investigations. *Ind. Eng. Chem. Res.* **2007**, *46* (7), 2020−2033.
(34) Kips, R.; Kristo, M.; Crowhurst, J.; Hutcheon, I.; Kristo, M. J.; Hutcheon, I. D. *Characterization of Uranium Oxyfluoride Particles for Nuclear Safeguards*; Annual Meeting Institute for Nuclear Materials Management, 2011.
(35) Su, J.; Wang, Z.; Pan, D.; Li, J. Excited States and Luminescent Properties of UO_2F_2 and Its Solvated Complexes in Aqueous Solution. *Inorg. Chem.* **2014**, *53* (14), 7340−7350.
(36) Görller-Walrand, C.; Gos, M. P.; D'Olieslager, W. The Luminescence Spectra of UF_4 and UCl_4. *Radiochim. Acta* **1993**, *62* (1−2), 55−60.
(37) Wang, Q.; Pitzer, R. M. Structure and Spectra of UO_2F_2 and Its Hydrated Species. *J. Phys. Chem. A* **2001**, *105* (36), 8370−8375.
(38) Xie, J.; Wang, Y.; Liu, W.; Yin, X.; Chen, L.; Zou, Y.; Diwu, J.; Chai, Z.; Albrecht-Schmitt, T. E.; Liu, G.; Wang, S. Highly Sensitive Detection of Ionizing Radiations by a Photoluminescent Uranyl Organic Framework. *Angew. Chem.* **2017**, *129* (26), 7608−7612.
(39) Wani, B. N.; Patwe, S. J.; Rao, U. R. K.; Venkateswarlu, K. S. Fluorination of Oxides of Uranium and Thorium by Ammonium Hydrogenfluoride. *J. Fluorine Chem.* **1989**, *44* (2), 177−185.
(40) Benz, R.; Douglass, R. M.; Kruse, F. H.; Penneman, R. A. Preparation and Properties of Several Ammonium Uranium(IV) and Ammonium Plutonium(IV) Fluorides. *Inorg. Chem.* **1963**, *2* (4), 799−803.
(41) Wani, B. N.; Rao, U. R. K. Interfacial Reaction between Ammonium Hydrogen Fluoride and Binary Oxides at Room Temperature. *Mater. Chem. Phys.* **1993**, *33* (1−2), 165−167.
(42) Bahri, C. N. A. C. Z.; Ismail, A. F.; Majid, A. A. Synthesis of Thorium Tetrafluoride (ThF_4) by Ammonium Hydrogen Difluoride (NH_4HF_2). *Nucl. Eng. Technol.* **2019**, *51* (3), 792−799.
(43) Silva, G. W. C.; Yeamans, C. B.; Cerefice, G. S.; Sattelberger, A. P.; Czerwinski, K. R. Synthesis and Nanoscale Characterization of $(NH_4)_4ThF_8$ and ThNF. *Inorg. Chem.* **2009**, *48* (13), 5736−5746.
(44) Poineau, F.; Silva, C. M.; Yeamans, C. B.; Cerefice, G. S.; Sattelberger, A. P.; Czerwinski, K. R. Structural Study of the Ammonium Octafluoroneptunate, $[NH_4]_4NpF_8$. *Inorg. Chim. Acta* **2016**, *448*, 93−96.
(45) Thomas, M. P.; Ullah, A.; Pham, R. H.; Djieutedjeu, H.; Selegue, J. P.; Guiton, B. S. Morphology Control in the Hydrothermal Synthesis of FeS Nanoplatelets. *Cryst. Growth Des.* **2020**, *20* (9), 5728−5735.
(46) Penn, R. L.; Banfield, J. F. Morphology Development and Crystal Growth in Nanocrystalline Aggregates under Hydrothermal Conditions: Insights from Titania. *Geochim. Cosmochim. Acta* **1999**, *63* (10), 1549−1557.
(47) Cho, S.; Jung, S. H.; Lee, K. H. Morphology-Controlled Growth of ZnO Nanostructures Using Microwave Irradiation: From Basic to Complex Structures. *J. Phys. Chem. C* **2008**, *112* (33), 12769−12776.
(48) Mellah, A.; Chegrouche, S.; Barkat, M. The Precipitation of Ammonium Uranyl Carbonate (AUC): Thermodynamic and Kinetic Investigations. *Hydrometallurgy* **2007**, *85* (2−4), 163−171.
(49) Sadeghi, M. H.; Outokesh, M.; Zare, M. H. Production of High Quality Ammonium Uranyl Carbonate from "Uranyl Nitrate + Carbonate" Precursor Solution. *Prog. Nucl. Energy* **2020**, *122*, No. 103270.
(50) Hanson, A. B.; Nizinski, C. A.; McDonald, L. W. Effect of Diel Cycling Temperature, Relative Humidity, and Synthetic Route on the Surface Morphology and Hydrolysis of α-U_3O_8. *ACS Omega* **2021**, *6* (28), 18426−18433.
(51) Hung, N. T.; Thuan, L. B.; Thuy, N. T.; Than, H. S.; Van Phuc, D.; Lee, J. Y.; Jyothi, R. K. Uranyl Ammonium Carbonate Precipitation and Conversion into Triuranium Octaoxide. *Heliyon* **2024**, *10* (4), No. e25930.
(52) Feldman, Y.; Frey, G. L.; Homyonfer, M.; Lyakhovitskaya, V.; Margulis, L.; Cohen, H.; Hodes, G.; Hutchison, J. L.; Tenne, R. Bulk Synthesis of Inorganic Fullerene-like MS_2 (M = Mo, W) from the Respective Trioxides and the Reaction Mechanism. *J. Am. Chem. Soc.* **1996**, *118* (23), 5362−5367.
(53) Vieira, L.; Martins Neto, J. D. R.; Ferreira, O. P.; Torresi, R. M.; Cordoba De Torresi, S. I.; Alves, O. L. Template Conversion of MoO_3 to MoS_2 Nanoribbons: Synthesis and Electrochemical Properties. *RSC Adv.* **2018**, *8* (53), 30346−30353.
(54) Woidy, P.; Karttunen, A. J.; Kraus, F. Uranyl Halides from Liquid Ammonia: $[UO_2(NH_3)_5]Cl_2{\cdot}NH_3$ and $[UO_2F_2(NH_3)_3]_2{\cdot}2NH_3$ and Their Decomposition Products $[UO_2Cl_2(NH_3)_3]$ and $[UO_2F_2(NH_3)_3]$. *Z. Anorg. Allg. Chem.* **2012**, *638* (12−13), 2044−2052.
(55) Lindstrom, R. M.; Ellis, W. P. Kinetics of the Hydrofluorination of Thorium Dioxide. *J. Chem. Phys.* **1965**, *43* (3), 994−997.
(56) Enriquez, E.; Wang, G.; Sharma, Y.; Sarpkaya, I.; Wang, Q.; Chen, D.; Winner, N.; Guo, X.; Dunwoody, J.; White, J.; Nelson, A.; Xu, H.; Dowden, P.; Batista, E.; Htoon, H.; Yang, P.; Jia, Q.; Chen, A. Structural and Optical Properties of Phase-Pure UO_2, α-U_3O_8, and α-

https://doi.org/10.1021/acsomega.4c02554
ACS Omega 2024, 9, 26380−26387

UO_3 Epitaxial Thin Films Grown by Pulsed Laser Deposition. *ACS Appl. Mater. Interfaces* **2020**, *12* (31), 35232−35241.
(57) Yoshihara, K.; Kanno, M.; Mukaibo, T. Preparation of Uranium Nitrides from Uranium Tetrafluoride. *J. Nucl. Sci. Technol.* **1968**, *5* (12), 643−647.
(58) Pomiro, F. J.; Gaviría, J. P.; Bohé, A. E.; De Micco, G. Thermodynamic Analysis of Uranium Oxides Fluorination with HF(g) and F_2(g). *J. Radioanal. Nucl. Chem.* **2020**, *324* (3), 1283−1292.
(59) Ellis, W. P. Hydrofluorination Kinetics of Doped Uranium Dioxide. *J. Nucl. Mater.* **1966**, *19* (2), 212−214.
(60) Louis-Jean, J.; Jang, H.; Swift, A. J.; Poineau, F. Thermal Analysis of Benzotriazolium Perrhenate and Its Implication to Rhenium Metal. *ACS Omega* **2021**, *6* (40), 26672−26679.

https://doi.org/10.1021/acsomega.4c02554
ACS Omega 2024, 9, 26380−26387